# Mapping Seasonal Flooding in Forested Wetlands Using Multi-Temporal Radarsat SAR

**Philip A. Townsend**

## Abstract

*Eleven Radarsat scenes imaged between 22 September 1996 and 28 February 1998 were analyzed to delineate flood inundation in the forests of the Roanoke River floodplain, North Carolina. Threshold $\sigma^\circ$ values distinguishing flooded from nonflooded forests were identified using classification trees. Data from 13 U.S. Geological Survey (USGS) wells located throughout the floodplain were used to validate the flood mapping with an overall accuracy of 93.5 percent. Images from both leaf-on and leaf-off periods were acceptable for detecting flooding, although the leaf-off scenes were classified with higher accuracy than were the leaf-on scenes (98.1 percent versus 89.1 percent). In addition, threshold $\sigma^\circ$ values were lower for leaf-on scenes. The results also indicate that Radarsat data can be used to detect minimal flood levels—sites with water stages between 10 cm below and 10 cm above the forest floor were classified with 90.6 percent accuracy. Radarsat data are effective and appropriate for flood inundation mapping in forests, regardless of season or water level.*

## Introduction

In the last decade, the analysis of synthetic aperture radar (SAR) imagery has become a valuable method for mapping flood inundation beneath forest canopies (Hess *et al.*, 1990; Wang *et al.*, 1995; Smith, 1997). The accurate delineation of inundation extent provides important information that can help guide management decisions and provide necessary data for application in hazards, hydrology, geomorphology, and landscape ecology research. SAR data are especially useful for flood detection over large areas where accurate flood mapping/modeling using other methods is difficult because hydrologic gage data are limited and surface topography is subtle. Further, in areas with dense forest cover and poor accessibility, SAR provides a remote method for mapping the spatial and temporal patterns of inundation that does not depend on detailed field observations or the availability of optical remote sensing data.

The advantages of radar for flood mapping arise from the ability of microwaves to (1) transmit through the atmosphere regardless of time of day or weather conditions and (2) penetrate forest canopies at certain frequencies and polarizations. The detection of flooding in forested wetlands using SAR results from double-bounce scattering of microwave energy from the water and trunks beneath the forest canopy (Figure 1). If the microwave energy is able to penetrate the canopy, it will reflect specularly from the still water on the surface and then again from the tree trunks back towards the SAR antenna (Richards *et al.*, 1987). Diffuse scattering from the ground in nonflooded areas reduces the returns from ground-trunk scattering, yielding dark image tones, whereas bright returns result from enhanced corner reflection between water and tree trunks (Hess *et al.*, 1990). SAR data collected at long wavelengths such as the L-band (1.3 GHz, 23.5 cm) and using HH polarization (horizontal receive and horizontal transmit) are especially useful for detecting flooded forests (Wang *et al.*, 1995). L-band SAR generally provides greater penetration of forest canopies than does the shorter C-band (5.3 GHz, 5.7 cm) because the wavelength is longer than leaf sizes within the forest canopy (Pope *et al.*, 1994; Wang *et al.*, 1995).

The majority of the results reported in the literature focus on the ability to map flooding in forested wetlands using data from L-HH SAR instruments such as those aboard Seasat, the Shuttle Imaging Radar missions (SIR-A, SIR-B, and SIR-C) and JERS-1 (Ormsby *et al.*, 1985; Place, 1985; Imhoff and Gesch, 1990; Hess and Melack, 1994; Hess *et al.*, 1995; Krohn *et al.*, 1983; Costa *et al.*, 1997a; Townsend and Walsh, 1998). Indeed, modeling efforts by Wang *et al.* (1995) confirm that SAR data at long wavelengths (L and P) and HH polarization are superior to C-band and VV polarized and cross-polarized SAR data for flood mapping. However, Wang *et al.* (1995) also showed that C-HH SAR exhibits some potential for mapping flooded forests. In contrast, C-VV SAR data such as from ERS-1/ERS-2 are not reliable for detecting flood inundation beneath forests (Kasischke and Bourgeau-Chavez, 1997; Townsend, 2001a) because canopy volume scattering contributes more to total backscatter at C-VV than do other wavelengths and polarizations (Wang *et al.*, 1995). No orbital L-band data are currently available; JERS-1, which was launched in 1992 with a design lifetime of two years, ceased operation in 1998, and Seasat failed in 1978 after 106 days of data collection.

In 1995, the Canadian Space Agency launched Radarsat, a C-HH orbital SAR that is capable of imaging the Earth at multiple incidence angles and several levels of spatial resolution. The wide coverage of Radarsat data has allowed the assessment of the capabilities of C-HH SAR for detecting flooding beneath forest canopies in a variety of environments. The results to date suggest that Radarsat data are useful for monitoring flooding in forests, exceeding the expectations suggested by Wang *et al.* (1995) and Hess *et al.* (1995). The abilities of Radarsat have been demonstrated in northern Australia (Milne *et al.*, 1998), throughout the Amazon Basin (Costa *et al.*, 1997b; Miranda *et al.*, 1997; Moreau and Bourrel, 1997) and North Carolina (the present study). However, none of the published studies have rigorously evaluated the accuracy of flood mapping using Radarsat, nor have they examined the capacity of Radarsat for mapping flood inundation during both leaf-on and leaf-off periods, which has also been identified as important (Kasischke and Bourgeau-Chavez, 1997).

The aim of this research is to quantitatively assess the

University of Maryland Center for Environmental Science, Appalachian Laboratory, 301 Braddock Road, Frostburg, MD 21532 (townsend@al.umces.edu).

Photogrammetric Engineering & Remote Sensing
Vol. 67, No. 7, July 2001, pp. 857–864.

0099-1112/01/6707–857$3.00/0

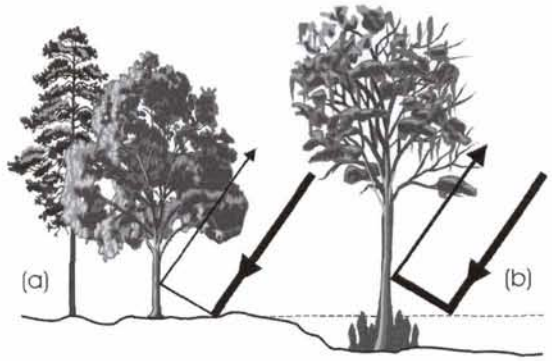


Figure 1. Trunk-ground interaction in a non flooded forest (a) and a flooded forest (b). Graphic adapted from Hess *et al.* (1990).

value of Radarsat imagery for mapping flooding beneath forest canopies at multiple stage/discharge levels and across seasons. This research is especially pertinent to resource managers and scientists who are interested in accurate, spatially explicit representations of flooding in lowland systems where subtle topographic variation limits the utility of digital elevation models for hydrologic studies. For ecologists, the "hydroperiod regime" (defined as the duration and spatial extent of flooding) is considered the most important abiotic factor influencing distribution and functioning of wetland forest types, but cannot be effectively modeled using standard digital elevation model (DEM) data. As a consequence, wetland scientists and resource managers have relied on very limited, site-intensive data to understand hydrology-vegetation interactions. By demonstrating the ability to operationally map seasonal patterns in flooding using Radarsat, the results presented here can provide scientists and decision-makers with a method to monitor flood duration and extent and to assess both the spatial and temporal impacts of water management policies.

## Study Area

The study area is the Roanoke River floodplain and adjacent uplands in northeastern North Carolina (Figure 2). The Roanoke River flows 225 kilometers from Roanoke Rapids Dam to its mouth at Albemarle Sound, and floodplain widths vary between 5 and 10 km. Near the mouth of the river, the study area also includes the basin of the Cashie River, which shares a series of distributaries at the conjoined mouths of the two rivers. The region consists of a diverse assemblage of bottomland hardwood and swamp forests that represent important habitat for nongame bird species (especially neotropical migrants, herons, egrets, and bald eagles). As a consequence, the Roanoke floodplain has been the subject of substantial conservation activities, including efforts by The Nature Conservancy, U.S. Fish and Wildlife Service, North Carolina Wildlife Resources Commission, and Georgia Pacific Corporation to protect over 25,000 ha of forest ecosystems.

These forested wetlands flood annually, with some locations on the floodplain inundated more than 11 months per year. Ecologically, the spatial variation in annual duration of inundation (hydroperiod) is one of the primary environmental factors controlling forest dynamics (Sharitz and Mitsch, 1993; Rice and Peet, 1997; Townsend, 2001b). As a consequence, researchers and environmental managers in the region are especially interested in determining the relationships between hydrology and forest composition and functioning because the floodplain has been influenced substantially by human activities such as the regulation of river flows through dam construc-

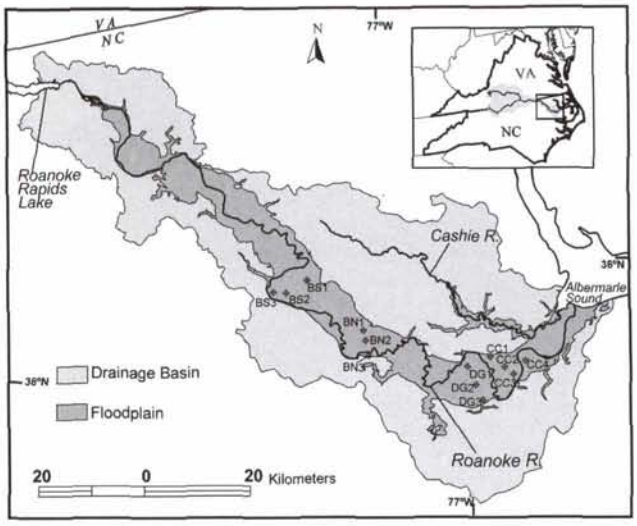


Figure 2. Location of the lower Roanoke River floodplain in eastern North Carolina. Also noted are the locations of the stage wells used to evaluate the results (Tables 3 and 4).

tion. A spatially explicit understanding of forest-hydrology dynamics on the floodplain therefore requires accurate delineation of flood inundation under multiple discharge scenarios. However, existing digital elevation models are insufficient to model differences in flood inundation at anything other than gross variations in discharge rates. For this reason, the analysis of SAR imagery represents an ideal tool for mapping flooding in these remote wetlands.

## Methods

### Image Processing

Eleven Radarsat scenes imaged between September 1996 and March 1998 were acquired and processed for the analyses (Table 1). The dates cover portions of three water years, and are representative of the range of discharge rates experienced on the Roanoke River during that period (Figure 3). The time period is bracketed by two ~1000 $m^3s^{-1}$ discharge events, the maximum discharge rate currently permitted from Roanoke

TABLE 1. RADARSAT SAR IMAGES AND ASSOCIATED DISCHARGE RATES

| Date | Beam Mode* | Incidence Angle (midswath) | Discharge (cfs)** | Discharge ($m^3s^{-1}$)** |
|---|---|---|---|---|
| 22 Sep 96 | S1 | 23.07 | 34720 | 983 |
| 02 Nov 96 | S2 | 27.49 | 6648 | 188 |
| 20 Dec 96 | S2 | 27.51 | 19600 | 555 |
| 26 Mar 97 | S2 | 27.51 | 14160 | 401 |
| 19 Apr 97 | S2 | 27.49 | 9244 | 262 |
| 06 Jun 97 | S2 | 27.51 | 7484 | 212 |
| 24 Jul 97 | S2 | 27.50 | 5484 | 155 |
| 17 Aug 97 | S2 | 27.51 | 5510 | 156 |
| 12 Oct 97 | S2 | 27.51 | 3372 | 95 |
| 21 Nov 97 | S2 | 27.50 | 7208 | 204 |
| 28 Feb 98 | S6 | 44.12 | 35420 | 1002 |

*Beam mode refers scale, resolution, and incidence angle position of a Radarsat scene. The "S" in the beam modes refers to "Standard Beam Mode" with a nominal area covered of 100 by 100 km, a nominal resolution of 30 m, and a pixel spacing of 12.5 m. The number refers to the pointing position, which is specified in the incidence angle column.
**Discharge rates are computed for each image as a five-day average (date of image and the four previous days).

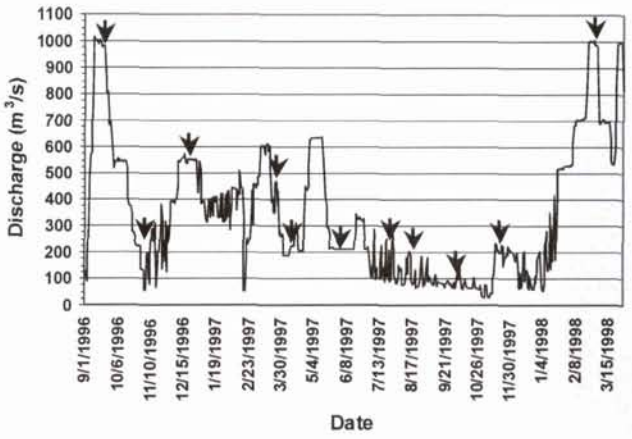


Figure 3. Hydrograph for the Roanoke River at Roanoke Rapids, September, 1996–March, 1998. Arrows indicate dates of Radarsat images listed in Table 1.

Rapids Dam. The remaining scenes include very dry conditions from the summer of 1997, as well as flood events that are typical of winter/spring moderate flows. Differences in flood inundation extent are evident on the images for these dates (Figure 4). Areas of bright tones in the floodplain represent flooded forests, whereas darker areas are not flooded. The river itself is apparent in most of the images, and has very dark tones due to near specular scattering from the river surface.

The Radarsat scenes were obtained from the Canadian Space Agency (CSA). Initial processing for all 11 scenes was performed at the Canadian Data Processing facility (CDPF). Calibration at the CDPF included antenna pattern removal and range fall-off correction. Absolute radiometric calibrations were implemented for the December 1996 and later Radarsat scenes by the CDPF. Absolute calibration of the 20 September 1996 and 02 November 1996 Radarsat scenes was applied following methods suggested by the CSA (Shepherd, 1998; Canada Centre for Remote Sensing, 1998). Sixteen-bit brightness values were converted to the radar scattering coefficient (sigma-nought, $\sigma^\circ$) using the PCI Works image processing software. All of the images were slant-to-ground range corrected and subsequently georeferenced to UTM coordinates using tie-points from 1:24,000-scale hydrography and roads layers. A second-order polynomial fit was applied, and pixel values were resampled using the nearest-neighbor method, resulting in a cumulative root-mean-square error (RMSE) of less than 15 m for all images. The image data were maintained in the 12.5-m pixel format in which they were distributed, although the actual ground range resolution of the scenes is closer to 22 m (range) by 27 m (azimuth). All of the images were smoothed using a 5 by 5 median filter for speckle reduction (Hess *et al.*, 1995).

#### Image Classification

The Radarsat images were classified into flooded and nonflooded forests using a binary recursive classifier (classification tree) in the S-Plus software. First, the images were masked using an existing land-cover classification generated from optical data (Landsat TM) for which a very high classification accuracy (greater than 90 percent) was reported (Townsend and Walsh, 2001). Nonforest areas (mostly agricultural fields and forest clearcuts) were not used for these analyses because returns from such areas exhibit a wider range of $\sigma^\circ$ than flooded and nonflooded forests. High variability in nonforested areas results from large differences in biomass levels, crop canopy structure, soil roughness, and soil moisture content.

Fifty-one training areas (an average size of 642 pixels, or ~10 ha) were identified on the image time series. Information from a variety of sources was used to select the training sites. Eleven upland forest sites were selected as representative of areas that never flood. Image interpretation and ancillary data (flood prediction models provided by Townsend and Walsh (1998)) were used to identify 16 permanently flooded locations. Other training areas were located across landforms that experience fluctuations in flooding. All training areas were evaluated individually for every image, with each site interpreted visually as either flooded or nonflooded. The exceptions to this were the two images at ~1000 $m^3s^{-1}$, for which flood inundation was identified using a flood prediction model at the same discharge rate (Townsend and Walsh, 1998). All of the training areas were unambiguously identified as either flooded or nonflooded on every image; any original training sites that could not be so identified were discarded from analysis. Table 2 lists the number of training areas classified as flooded and nonflooded for each date. None of the training areas overlapped with locations of the water stage wells that were later used to evaluate the mapping.

The training data were input into S-Plus, and classification trees were employed to identify threshold $\sigma^\circ$ values for differentiating between flooded and nonflooded forests. Classification trees (also known as decision trees) are fitted by binary recursive partitioning, in which data sets are consecutively divided into smaller subsets with increasing statistical homogeneity (Clark and Pregibon, 1993; see Friedl and Brodley (1997) for an application of decision trees to the classification of remotely sensed imagery). For this research, the training observations were split into groups of flooded versus nonflooded sites using $\sigma^\circ$ as the classification variable. Decision trees are desirable because they are less sensitive to nonlinearities in the input data than are methods that require assumptions of Gaussian distributions (as do many image classification techniques) (Clark and Pregibon, 1993; Venables and Ripley, 1994). The analysis used all pixels (a total of 32,744 for all 51 training sites). For each image, a single split between backscattering ($\sigma^\circ$) from flooded and nonflooded forests was identified (Table 2). Classification trees were not essential to identify the threshold $\sigma^\circ$, but the use of decision trees reduced the arbitrariness in selecting thresholds between classes. The value of $\sigma^\circ$ changed from scene to scene due to differences in incidence angle (especially 28 February 1998) and vegetation phenological status (leaf-on versus leaf-off). The threshold $\sigma^\circ$ is lower (i.e., darker tones on the image) for leaf-on periods due to increased canopy volume scattering. The relatively low misclassification rates listed in Table 2 indicate preliminarily that the threshold $\sigma^\circ$ values were appropriate for mapping flooded and nonflooded forests. It is worth noting that misclassification of training pixels was most likely a consequence of the residual effects of image speckle. Following classification of the images, a 5 by 5 majority filter was passed over the classification to reduce the remaining effects of speckling on the classified maps.

#### Classification Evaluation

The classification was evaluated using data from 13 stage wells located throughout the floodplain (Figure 2). The wells were installed by the U.S. Geological Survey in 1996 with some guidance from the author and environmental managers in the region, and most were fully operational by early 1997. Data from wells such as these represent the only ancillary information available to rigorously evaluate the accuracy of the classification. Because of the expense of installing and maintaining such wells, there cannot be a large enough set of observations to satisfy traditional recommendations for validation sample size (e.g., Congalton and Green, 1998). This is acknowledged as a possible limitation in the accuracy assessment of this study; however, it is rare that even 13 continuously recording stage

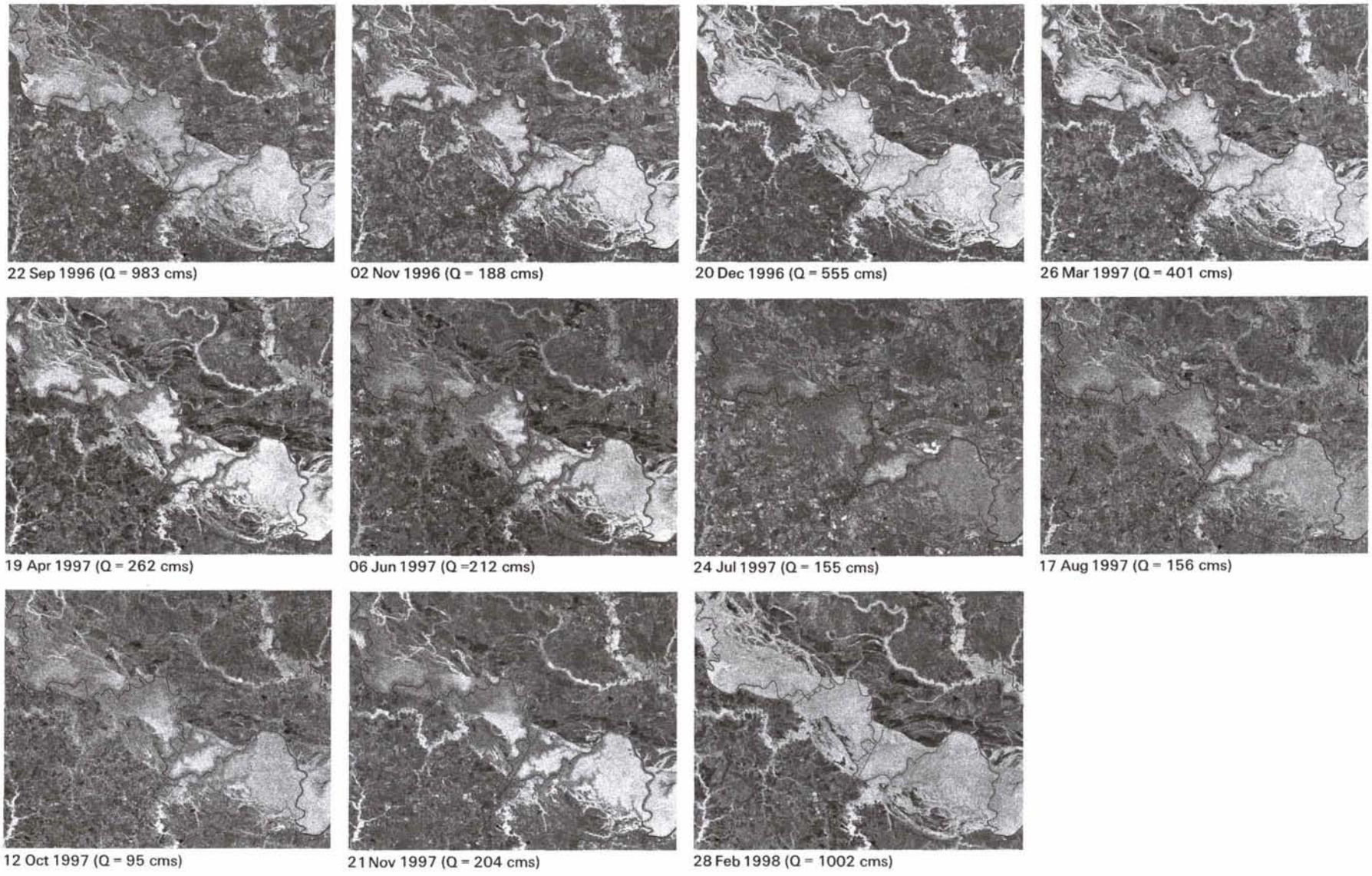


Figure 4. Subsets of Radarsat images used in the research. Discharge rates are listed for each date. Image scale is 1:555,556.

TABLE 2. NUMBER OF TRAINING SITES IDENTIFIED AS FLOODED OR NONFLOODED ON EACH IMAGE AND THRESHOLD BACKSCATTER COEFFICIENTS ($\sigma^\circ$) USED TO CLASSIFY FLOODED AND NONFLOODED FORESTS

| Date | Nonflooded | Flooded | Threshold $\sigma^\circ$ (dB) | Misclassification Rate |
|---|---|---|---|---|
| 22 Sep 96 | 12 | 39 | −5.75 | 0.066 |
| 02 Nov 96 | 25 | 26 | −4.16 | 0.007 |
| 20 Dec 96 | 20 | 31 | −4.21 | 0.010 |
| 26 Mar 97 | 22 | 29 | −4.28 | 0.027 |
| 19 Apr 97 | 25 | 26 | −5.76 | 0.026 |
| 06 Jun 97 | 26 | 25 | −6.17 | 0.068 |
| 24 Jul 97 | 33 | 18 | −5.1 | 0.073 |
| 17 Aug 97 | 33 | 18 | −5.88 | 0.065 |
| 12 Oct 97 | 35 | 16 | −5.46 | 0.033 |
| 21 Nov 97 | 33 | 18 | −4.23 | 0.046 |
| 28 Feb 98 | 12 | 39 | −8.21 | 0.054 |

wells are available on a floodplain. For the 11 images used in this study, a total of 108 flood-stage observations were available and considered reliable by the USGS, and it is upon these observations that the effectiveness of the methods and accuracy of the maps were evaluated.

A military Global Positioning System (GPS) receiver with spatial error less than 10 m was used to record the locations of the stage wells. The coordinates were input into a geographic information system and were overlaid on the classified images to assess the accuracy of the mapping. Stage data were evaluated in reference to a 3- by 3-pixel window (37.5 m by 37.5 m) around the location of each well on the classified maps. A majority rule was used to assess whether the window for each well was mapped as flooded or nonflooded. Actual flood status was interpreted from the average daily stage height information for each well, with positive values (water table above the surface) indicating flooded locations and negative values (water table below the surface) representing nonflooded sites (Table 3). Water levels at the surface (stage height = 0.0) were treated as flooded. Water levels between 10 cm above and 10 cm below the surface were treated as flooded or nonflooded, respectively, although it was considered possible that microtopographic variation would be sufficient to cause errors in flood inundation mapping within the given 3- by 3-pixel area. The implications for mapping flooding at low levels are examined in detail in the following sections.

## Results and Discussion

### Detection of Flooding Using Radarsat

Table 4 reports the evaluation of the well data for each image date based on the interpretation of stage heights (Table 3) and the classified maps. Incorrect observations are denoted on Table 4 with an "x," and a "*" is used to identify the well observations interpreted as "low levels" of flooding, where water stage was between 10 cm above and 10 cm below the surface.

The overall classification accuracy was high. Across all eleven dates, 101 of the 108 well observations (93.5 percent) were correctly mapped (Table 5). Flooded sites were mapped with slightly higher accuracy than were nonflooded locations (95 percent versus 91.67 percent). Flooding is more accurately mapped because of the distinct and continuous enhanced returns from flooded forests, in contrast to nonflooded forests, which exhibit a greater range in backscatter due to differences in forest structure, surface roughness, surface moisture content, and other factors (Townsend, 2001a; Townsend, 2001c). Nevertheless, flooded and nonflooded forests were both detected accurately. On only one date, 24 July 1997, was more than one well mapped incorrectly. This is addressed in greater detail in the discussion of differences between leaf-on and leaf-off scenes.

Based on these analyses, the C-HH SAR data from Radarsat appear to be appropriate for accurately mapping inundation in the forests of the southeastern U.S. It is likely that, in tropical regions with taller, more complex forests and higher year-round leaf area index (LAI) values, such as those discussed by Wang *et al.* (1995) and Hess *et al.* (1995), Radarsat may be less effective for mapping subcanopy flooding.

### Leaf-On versus Leaf-Off

The accuracy assessment data were evaluated to determine whether phenological status influenced the ability to accurately detect flood inundation beneath forest canopies. For the purposes of this study, five dates were treated as leaf-on (September, 1996, and June, July, August, and October, 1997) and six dates were considered leaf-off (November and December 1996; March, April, and November, 1997; and February, 1998). These are not unambiguous distinctions, because some senescence was likely on both the September, 1996 and October, 1997 images. In addition, some leaf-out would certainly have occurred by 19 April 1997, but any new leaves were likely still small in mid-April. In general, leaf-out also tends to occur at later dates on wet sites of the floodplain (Townsend and Walsh, 2001).

The differences between leaf-on and leaf-off images for interpretation of flooding on Radarsat images is most notable by contrasting the 22 September 1996 image with the 28 February 1998 scene (Figure 4). Discharge levels on the river were nearly identical on the two dates (Table 1; see also stage heights in Table 3), meaning that inundation extent was comparable between dates. However, flooded areas are much more readily interpreted visually from the leaf-off scene (February) than from the leaf-on scene (September). Despite this, the flooded

TABLE 3. WATER STAGE LEVEL ABOVE FLOODPLAIN SURFACE (METERS)

| | Well Location | | | | | | | | | | | | |
|---|---|---|---|---|---|---|---|---|---|---|---|---|---|
| Date | CC-1 | CC-2 | CC-3 | CC-4 | DG-1 | DG-2 | DG-3 | BN-1 | BN-2 | BN-3 | BS-1 | BS-2 | BS-3 |
| 22 Sep 1996 | | 0.86 | 0.72 | 0.33 | 1.08 | 1.27 | 1.08 | | | 1.32 | | | |
| 02 Nov 1996 | | 0.15 | 0.13 | 0.05 | 0.09 | 0.39 | 0.57 | | | −0.05 | | | |
| 20 Dec 1996 | | 0.25 | 0.16 | −0.16 | 0.60 | 0.79 | 0.66 | | 2.28 | 0.97 | | | |
| 26 Mar 1997 | | 0.22 | 0.17 | 0.08 | 0.50 | 0.71 | 0.63 | | | 0.69 | | | |
| 19 Apr 1997 | | −0.19 | −0.09 | −0.27 | −0.03 | 0.11 | 0.54 | 0.10 | | −0.13 | | | |
| 06 Jun 1997 | 0.00 | 0.09 | 0.08 | 0.05 | −0.02 | 0.16 | 0.53 | 0.12 | | −0.10 | | 0.24 | 0.21 |
| 24 Jul 1997 | −0.08 | 0.02 | −0.02 | −0.06 | −0.24 | 0.00 | 0.34 | 0.09 | 0.56 | −0.23 | −0.95 | −0.45 | −1.17 |
| 17 Aug 1997 | −0.48 | −0.03 | −0.05 | −0.07 | −0.80 | −0.35 | 0.22 | 0.01 | −0.11 | −0.68 | | −0.77 | −1.57 |
| 12 Oct 1997 | −0.29 | −0.07 | −0.09 | −0.14 | −1.02 | −0.30 | 0.17 | −0.02 | −0.57 | −0.85 | | −0.85 | −1.87 |
| 21 Nov 1997 | −0.02 | −0.07 | −0.08 | −0.11 | −0.41 | 0.03 | 0.30 | −0.01 | 0.29 | −0.40 | −1.14 | −0.67 | −1.88 |
| 28 Feb 1998 | 0.02 | 0.81 | 0.63 | 0.38 | 0.98 | | | 1.89 | 2.64 | 1.31 | 0.75 | 2.11 | |

Positive values indicate flood depth and negative values indicate depth to water table. Empty cells indicate missing data.

TABLE 4. MAP CLASSIFICATION FOR FLOODPLAIN GAGES LISTED IN TABLE 3

| Date | Well Location | | | | | | | | | | | | |
|---|---|---|---|---|---|---|---|---|---|---|---|---|---|
| | CC-1 | CC-2 | CC-3 | CC-4 | DG-1 | DG-2 | DG-3 | BN-1 | BN-2 | BN-3 | BS-1 | BS-2 | BS-3 |
| 22 Sep 1996 | | F | F | F | F | F | F | | | F | | | |
| 02 Nov 1996 | | F | F | F* | F* | F | F | | | N* | | | |
| 20 Dec 1996 | | F | F | N | F | F | F | | F | F | | | |
| 26 Mar 1997 | | F | F | F* | F | F | F | | | F | | | |
| 19 Apr 1997 | | N | N* | N | N* | F | F | F* | | N | | | |
| 06 Jun 1997 | F* | F* | F* | F* | N* | F | F | F | | N* | | F | Nx |
| 24 Jul 1997 | F*x | F* | F*x | F*x | N | F* | F | F* | Nx | N | N | N | N |
| 17 Aug 1997 | N | N* | N* | N* | N | N | F | F* | N | N | | N | N |
| 12 Oct 1997 | N | N* | N* | N | N | N | Nx | N* | N | N | | N | N |
| 21 Nov 1997 | N* | N* | N* | N | N | F* | F | F* | Nx | N | N | N | N |
| 28 Feb 1998 | F* | F | F | F | F | | | F | F | F | F | F | |

N indicates that the well location was mapped as nonflooded on the Radarsat scene for that date.
F indicates that the well location was mapped as flooded on the Radarsat scene for that date.
* indicates that the stage level for that date was between 10 cm above and 10 cm below the floodplain surface.
x indicates that the observation was incorrectly mapped (see Table 3).

TABLE 5. CLASSIFICATION ACCURACY OF FLOODED AND NONFLOODED FORESTS

| | Reference Data (from floodplain stage observations) | | | | | | | | |
|---|---|---|---|---|---|---|---|---|---|
| | All Images | | | Leaf-Off Images | | | Leaf-On Images | | |
| Map Class | Flooded | Nonflooded | % Correct | Flooded | Nonflooded | % Correct | Flooded | Nonflooded | % Correct |
| Flooded | 57 | 3 | 95.00 | 36 | 0 | 100.00 | 21 | 3 | 87.50 |
| Nonflooded | 4 | 44 | 91.67 | 1 | 16 | 94.12 | 3 | 28 | 90.32 |
| Overall | | | 93.52 | | | 98.11 | | | 89.09 |

areas with darker tones on the September image exhibited a statistical difference from nonflooded areas, and those differences are also visually apparent when comparing floodplain forests to adjacent upland forests on the September image. This suggests that flooded areas can still be mapped accurately from the leaf-on image; however, the visual distinction is not as pronounced.

Quantitative differences between leaf-on and leaf-off scenes are also notable from the threshold $\sigma^\circ$ levels that were used to distinguish flooded and nonflooded forests (Table 2). With the exception of the 28 February 1996 scene (discussed in the section on incidence angle below), the leaf-on scenes have lower threshold backscattering coefficients (i.e., darker tones on the images, around $-4.2$ dB for leaf-off versus $-5.1$ dB and lower for leaf-on). The generally lower thresholds and the wider variability in the threshold $\sigma^\circ$ values indicates that leaf-on forests yield at least a 1 dB lower enhancement of backscattering due to flooding than do leaf-off forests.

Table 5 indicates the differences in classification accuracy between leaf-on and leaf-off dates. Flooded and nonflooded forests were mapped accurately regardless of season. However, the overall accuracy for the leaf-off scenes was substantially higher than for leaf-on images (98.1 percent versus 89.1 percent). Flooded and nonflooded forests were both mapped very accurately on the leaf-off scenes, and, in fact, all flooded wells were correctly mapped on the leaf-off scenes. These results confirm observations that the lower leaf area experienced during senescent periods improves the ability to distinguish flooded and nonflooded forests (e.g., Kasischke and Bourgeau-Chavez, 1997). Inaccuracies on the leaf-on images result from the effects of increased canopy attenuation and volume scattering at short (C-band, 5.7 cm) wavelengths. This is the primary reason that long-wavelength SAR data (especially L-band, 23.5 cm) are preferable for flood mapping beneath forest canopies (Richards *et al.*, 1987; Hess *et al.*, 1990; Wang *et al.*, 1995). Nevertheless, because L-band data are not currently available from orbital systems, C-HH data such as from Radarsat remain the best tool for mapping flooded forests. At present, the only SAR satellite in planning that will carry an L-band SAR sensor is ALOS (Japan, to be launched in 2002 or later). Both Radarsat-2 (scheduled for launch by Canada in 2003) and Envisat-1 (scheduled for launch by the European Space Agency in 2001) will have the ability to collect co-polarized data in addition to like-polarized data, but only at the C-band frequency.

Finally, it is worth noting that the highest misclassification rate for the flood mapping was on the 24 July 1997 image (four of 13 wells mapped incorrectly, total accuracy 69.2 percent). Although one must be careful not to infer too much from the small sample of validation points, it is reasonable to assume that the relative inaccuracy of the classification for 24 July results from the scene having been imaged near the height of leaf flush. On this scene, the forests were most fully leafed-out compared to the other dates, with maximum leaf vigor and minimum senescence. It should also be noted that three of the four wells were inaccurately mapped as flooded. At all three, water tables were within 10 cm of the surface, implying that depending on microtopography, some of the area surrounding those wells may in fact have had standing water above the forest floor.

#### Incidence Angle

Hess *et al.* (1990) and Wang *et al.* (1995) indicate that steep incidence angles (less than 35°) are preferable to shallow angles (greater than 35°) for mapping flooded forests. This generalization can be attributed to increased canopy volume scattering as a consequence of longer path lengths through the canopy at shallow incidence angles. However, as noted by Hess *et al.* (1990), this angular dependence has not been conclusively confirmed in the literature. The angular dependence of increased backscattering from flooded forests depends largely on forest type and structure, which in turn affect attenuation/volume scattering (Hess *et al.*, 1990). A comprehensive examination of the effects of incidence angle on the capability to detect flooded forests using Radarsat is not possible with the data used

TABLE 6. CLASSIFICATION ACCURACY OF FLOODED AND NONFLOODED FORESTS FOR OBSERVATIONS WHERE THE WATER STAGE WAS BETWEEN 10 CM ABOVE AND 10 CM BELOW THE FLOODPLAIN SURFACE

| | Reference Data (from floodplain stage observations) | | | | | | | | |
|---|---|---|---|---|---|---|---|---|---|
| | All Images | | | Leaf-Off Images | | | Leaf-On Images | | |
| Map Class | Flooded | Nonflooded | % Correct | Flooded | Nonflooded | % Correct | Flooded | Nonflooded | % Correct |
| Flooded | 15 | 3 | 83.33 | 7 | 0 | 100.00 | 8 | 3 | 72.73 |
| Nonflooded | 0 | 14 | 100.00 | 0 | 6 | 100.00 | 0 | 8 | 100.00 |
| Overall | | | 90.63 | | | 100.00 | | | 84.21 |

in this study. A factorial design controlling for flood levels and phenology would be required to properly address angular effects. However, a few general trends can be noted in the data. First, flooding is easily identified on the February 1998 scene (Figure 4), which had the shallowest incidence angle of any of the scenes used in this research (44.1° at mid-swath). The steepest incidence angle was for the September 1996 scene (23.1° at mid-swath); although flooding is readily detectable on this scene, it is not directly comparable to the February scene due to phenological differences, as noted previously. The remaining scenes were imaged in Radarsat S2 mode (approximately 27.5° midswath), and in general the contrast between flooded and nonflooded forests appears greater on these than on the February image (compare 20 December 1996 and 28 February 1998 on Figure 4). The best quantitative assessment of incidence angle effects is provided by Table 2, in which it is notable that a much lower threshold $\sigma^{\circ}$ (−8.21 dB) was required to detect flooded forests on the shallow angle image (February 1998) than on the images with steeper incidence angles (e.g., 20 December, −4.21 dB). This suggests a 4-dB difference in the level of enhanced backscattering between flooded forests imaged in the S2 and S6 modes.

### Low Flooding

A final issue regarding the detectability of flooding in forests is depth of flooding. Flood inundation may not be consistently detected in areas where water levels are at or near the surface. At low flood levels, factors such as microtopographic relief and the presence of features that increase surface roughness (herbaceous/woody understory vegetation, cypress knees, coarse woody debris) can be expected to reduce the usual enhanced backscattering through increases in diffuse scattering at the surface. Nevertheless, from an applied perspective, it is important to detect low levels of inundation, especially in areas where topographic relief is subtle.

To examine the detectability of low flooding using Radarsat, the stage data and classifications were reevaluated for only those observations at which water levels were between 10 cm above and 10 cm below the surface. As with the previous analyses, all observations with stages at or above 0.0 were considered flooded whereas those below 0.0 were considered nonflooded. This more restricted evaluation demonstrates that Radarsat data can be used to accurately detect flooding even under conditions where water levels are at or near the surface (Table 6). Overall accuracy was 90.6 percent for all images, with nonflooded sites (water level −0.10 to −0.01 m) mapped more accurately than flooded sites (0.0 m to +0.10 m). All of the sites were accurately classified on the leaf-off images (100 percent accuracy), whereas the accuracy of the leaf-on, low flooding sites was 84.21 percent. This follows the same trend as reported for the entire data set, in which flooding beneath forests is mapped most accurately on leaf-off images, but is nevertheless mapped at acceptable levels of accuracy on the leaf-on scenes.

These results show that Radarsat data are effective for discriminating between flooded and nonflooded forests at relatively low levels of inundation, regardless of microsite variation.

## Conclusions

This research confirms that Radarsat SAR data can be used operationally to map flooded forests in temperate regions regardless of season and water stage. Although there are notable differences between leaf-on and leaf-off images in the accuracy of flood detection and in the threshold backscatter coefficients used to distinguish flooded/nonflooded forests, the methods nevertheless proved suitable for all seasons. Moreover, the high classification accuracy for sites with shallow flood depths demonstrates the overall robustness of Radarsat data for flood inundation mapping. Based on these results, it is reasonable to suggest that time series of Radarsat images can be used to quantitatively assess hydrological gradients in forested wetlands. The methods used here are suitable for validating hydrologic models of floodplain inundation, for providing independent verification of the hydrologic effects of altered flow regimes, and for evaluating the relationships between hydroperiod regime and ecosystem functioning.

## Acknowledgments

Support for this research was provided by the Application Development and Research Opportunity (ADRO) program of Radarsat/Canadian Space Agency (Project 476) and The Nature Conservancy. Thanks to Doug Walters at the U.S. Geological Survey for providing data support, and to Jeff Horton, Este Stifel, and Sam Pearsall at The Nature Conservancy for their efforts in securing the installation of the stage wells. Thanks also to Clayton Kingdon, Yancy Craft, and Jane Foster for graphic design. Special thanks to Steve Walsh at the University of North Carolina and Sam Pearsall at TNC for their support of this research. This paper is Scientific Series Contribution Number 3392-AL, University of Maryland Center for Environmental Science.

## References

Canada Centre for Remote Sensing, 1998. *Estimation of Change in Radar Brightness between Uncalibrated and Calibrated CDPF Products*, Technical Note, Canada Centre for Remote Sensing, Ottawa, Canada, 5 p.

Clark, L.A., and D. Pregibon, 1993. Tree-based models, *Statistical Models in S* (J.M. Chambers and T.J. Hastie, editors), Chapman and Hall, New York, N.Y., pp. 377–419.

Congalton, R.G., and K. Green, 1998. *Assessing the Accuracy of Remotely Sensed Data: Principals and Practices*, Lewis Publishers, Boca Raton, Florida, 137 p.

Costa, M.P.F., E.M.L.M. Novo, F.J. Ahern, and R.W. Pietsch, 1997a. Seasonal dynamics of the Amazon floodplain through RADAR eyes: Lago Grande de Monte Alegre case study, *RADARSAT for Amazonia: Results of ProRADAR Investigations* (F.J. Ahern, editor), Canada Centre for Remote Sensing, Natural Resources Canada, Ottawa, Ontario, Canada, pp. 163–171.

Costa, M.P.F., E.M.L.M. Novo, F. Mitsuo II, J.E. Mantovani, M.V. Ballester, and F.J. Ahern, 1997b. Classification of floodplain habitats (Lago Grande, Brazilian Amazon) with RADARSAT and JERS-1 data, *RADARSAT for Amazonia: Results of ProRADAR Investigations* (F.J. Ahern, editor), Canada Centre for Remote Sensing, Natural Resources Canada, Ottawa, Ontario, Canada, pp. 149–161.

Friedl, M.A., and C.E. Brodley, 1997. *Decision tree classification of land cover from remotely sensed data*, *Remote Sensing of Environment*, 61(3):399–409.

Hess, L.L., and J.M. Melack, 1994. Mapping wetland hydrology and vegetation with synthetic aperture radar, *International Journal of Ecology and Environmental Sciences*, 20:197–205.

Hess, L.L., J.M. Melack, and D.S. Simonett, 1990. Radar detection of flooding beneath the forest canopy: A review, *International Journal of Remote Sensing*, 11(7):1313–1325.

Hess, L.L., J.M. Melack, S. Filoso, and Y. Wang, 1995. Delineation of inundated area and vegetation along the Amazon floodplain with the SIR-C synthetic-aperture radar, *IEEE Transactions on Geoscience & Remote Sensing*, 33(4):896–904.

Imhoff, M.L., and D.B. Gesch, 1990. The derivation of a sub-canopy digital terrain model of a flooded forest using synthetic aperture radar, *Photogrammetric Engineering & Remote Sensing*, 56(8):1155–1162.

Kasischke, E.S., and L.L. Bourgeau-Chavez, 1997. Monitoring South Florida wetlands using ERS-1 SAR imagery, *Photogrammetric Engineering & Remote Sensing*, 63(3):281–291.

Krohn, M.D., N.M. Milton, and D.B. Segal, 1983. SEASAT synthetic aperture radar (SAR) response to lowland vegetation types in eastern Maryland and Virginia, *Journal of Geophysical Research*, 88(C3):1937–1952.

Milne, A.K., G. Horne, and C.M. Finlayson, 1998. Monitoring wetlands inundation patterns using RADARSAT multitemporal data, *RADARSAT ADRO Final Symposium*, 13–15 October, Montréal, Quebec, available on CDROM or at URL, pp. xxx–xxx.

Miranda, F.P., L.E.N. Fonseca, C.H. Beisl, Å. Rosenqvist, and M.D.M.A.M. Figueiredo, 1997. Seasonal mapping of flooding extent in the vicinity of the Balbina Dam (Central Amazonia) using RADARSAT-1 and JERS-1 SAR data, *RADARSAT for Amazonia: Results of ProRADAR Investigations* (F.J. Ahern, editor), Canada Centre for Remote Sensing, Natural Resources Canada, Ottawa, Ontario, Canada, pp. 187–191 (plus figures).

Moreau, S., and L. Bourrel, 1997. Hydrogeodynamics of the wetlands in the Bolivian Amazon basin, *RADARSAT for Amazonia: Results of ProRADAR Investigations* (F.J. Ahern, editor), Canada Centre for Remote Sensing, Natural Resources Canada, Ottawa, Ontario, Canada, pp. 193–198 (plus figures).

Ormsby, J.P., B.J. Blanchard, and A.J. Blanchard, 1985. Detection of lowland flooding using active microwave systems, *Photogrammetric Engineering & Remote Sensing*, 51(3):317–328.

Place, J.L., 1985. Mapping of forested wetland: use of Seasat radar images to complement conventional sources, *Professional Geographer*, 37(4):463–469.

Pope, K.O., J.M. Rey-Benayaas, and J.F. Paris, 1994. Radar remote sensing of forest and wetland ecosystems in the Central American tropics, *Remote Sensing of Environment*, 48:205–219.

Rice, S.K., and R.K. Peet, 1997. *Vegetation of the Lower Roanoke River Floodplain*, The Nature Conservancy, Durham, North Carolina, 154 p.

Richards, J.A., P.W. Woodgate, and A.K. Skidmore, 1987. An explanation of enhanced radar backscatter from flooded forests, *International Journal of Remote Sensing*, 8(7):1093–1100.

Sharitz, R.R., and W.J. Mitsch, 1993. Southern floodplain forests, *Biodiversity of the Southeastern United States: Lowland Terrestrial Communities* (W.H. Martin, S.G. Boyce, and A.C. Echternacht, editors), John Wiley and Sons, New York, N.Y., pp. 311–372.

Shepherd, N., 1998. *Extraction of Beta Nought and Sigma Nought from RADARSAT CDPF Products*, Report No. AS97-5001, ALTRIX Systems, Inc., Ottawa, Ontario, Canada, 13 p.

Smith, L.C., 1997. Satellite remote sensing of river inundation area, stage, and discharge: A review, *Hydrological Processes*, 11(10):1427–1439.

Townsend, P.A., 2001a. Relationships between forest structure and the detection of flood inundation in forested wetlands using C-band SAR, *International Journal of Remote Sensing* (in press).

———, 2001b. Relationships between vegetation patterns and hydroperiod on the Roanoke River floodplain, North Carolina, *Plant Ecology* (in press).

———, 2001c. Estimating forest structure in wetlands using multitemporal SAR, *Remote Sensing of Environment* (in press).

Townsend, P.A., and S.J. Walsh, 1998. Modeling floodplain inundation using an integrated GIS with radar and optical remote sensing, *Geomorphology*, 21(3–4):295–312.

———, 2001. Remote sensing of forested wetlands: application of multitemporal and multispectral satellite imagery to determine plant community composition and structure in Southeastern USA, *Plant Ecology* (in press).

Venables, W.N., and B.D. Ripley, 1994. *Modern Applied Statistics with S-Plus*, Springer-Verlag, New York, N.Y., 462 p.

Wang, Y., L.L. Hess, S. Filoso, and J.M. Melack, 1995. Understanding the radar backscattering from flooded and nonflooded Amazonian forests: Results from canopy backscatter modeling, *Remote Sensing of Environment*, 54(3):324–332

(Received 14 February 2000; accepted 28 November 2000; revised 11 December 2000)